

RESEARCH ARTICLE | MARCH 01 2024

Programmable photonic system for quantum simulation in arbitrary topologies

Ben Bartlett  ; Olivia Y. Long   ; Avik Dutt  ; Shanhui Fan 

 Check for updates

APL Quantum 1, 016102 (2024)

<https://doi.org/10.1063/5.0181151>



APL Quantum

First Articles Online

No Article Processing Charges for Submissions
Through December 31, 2024

Read Now


AIP
Publishing

Programmable photonic system for quantum simulation in arbitrary topologies

Cite as: APL Quantum 1, 016102 (2024); doi: 10.1063/5.0181151

Submitted: 14 October 2023 • Accepted: 1 February 2024 •

Published Online: 23 February 2024



Ben Bartlett,^{1,a)} Olivia Y. Long,^{1,b)} Avik Dutt,^{2,3} and Shanhui Fan^{4,c)}

AFFILIATIONS

¹ Department of Applied Physics, Stanford University, Stanford, California 94305, USA

² Department of Mechanical Engineering, and Institute for Physical Science and Technology (IPST), University of Maryland, College Park, Maryland 20742, USA

³ National Quantum Laboratory (QLab) at Maryland, College Park, Maryland 20742, USA

⁴ Department of Electrical Engineering, Stanford University, Stanford, California 94305, USA

^{a)}Current address: PsiQuantum, Palo Alto, CA 94304, USA.

^{b)}Author to whom correspondence should be addressed: olong@stanford.edu

^{c)}E-mail: shanhui@stanford.edu

ABSTRACT

Synthetic dimensions have generated great interest for studying many types of topological, quantum, and many-body physics, and they offer a flexible platform for simulation of interesting physical systems, especially in high dimensions. In this paper, we describe a programmable photonic device capable of emulating the dynamics of a broad class of Hamiltonians in lattices with arbitrary topologies and dimensions. We derive a correspondence between the physics of the device and the Hamiltonians of interest, and we simulate the physics of the device to observe a wide variety of physical phenomena, including chiral states in a Hall ladder, effective gauge potentials, and oscillations in high-dimensional lattices. Our proposed device opens new possibilities for studying topological and many-body physics in near-term experimental platforms.

© 2024 Author(s). All article content, except where otherwise noted, is licensed under a Creative Commons Attribution (CC BY) license (<http://creativecommons.org/licenses/by/4.0/>). <https://doi.org/10.1063/5.0181151>

04 April 2024 22:16:24

The emerging concept of synthetic dimensions in photonics has generated great interest for topological physics,^{1–5} optimization,^{6–9} and quantum simulation and computation.^{10–17} Synthetic dimensions are formed by controlling couplings between degrees of freedom of a system, either by repurposing the usual geometric dimensions, such as space¹⁸ or time,^{6–8,19–23} or by augmenting these dimensions with internal degrees of freedom, such as frequency,^{11,24–27} spin,^{1,28–30} or orbital angular momentum.^{31,32} Since couplings in synthetic dimensions can be dynamically reconfigured and are not fixed by a physical structure, one can scalably implement high-dimensional lattices with complex topologies, making this an ideal platform for quantum simulation.

In this theoretical work, we describe a programmable photonic device capable of simulating the dynamics of interacting bosons in lattices with arbitrary dimensions, topologies, and connectivities using a synthetic time dimension. A large class of prototypical condensed matter Hamiltonians can be described by local two-body interactions on an arbitrary lattice. This class of

Hamiltonians, which includes tight-binding models, the Hubbard and Bose-Hubbard models and their various extensions,³³ and the Harper-Hofstadter-Hubbard model,³⁴ can, in general, be described as (using $\hbar = 1$ throughout this paper),

$$\hat{H} = - \sum_{\langle m,n \rangle} \left(\kappa_{mn} e^{i\alpha_{mn}} \hat{a}_m^\dagger \hat{a}_n + \text{H.c.} \right) + \mu \sum_m \hat{a}_m^\dagger \hat{a}_m + U \sum_m \hat{a}_m^\dagger \hat{a}_m^\dagger \hat{a}_m \hat{a}_m, \quad (1)$$

where κ_{mn} and α_{mn} , respectively, denote the tunneling coefficients and phases between connected sites $\langle m, n \rangle$, \hat{a}_m^\dagger creates a boson at site m , μ is the chemical potential, and U is the Hubbard interaction strength. The first term describes the tunneling of a particle between sites m and n , with a complex tunneling strength with amplitude κ_{mn} and phase α_{mn} ; the second term sets the energy per particle μ ; and the third term is an on-site interaction potential with strength U , which is active when a site contains more than one particle. This very general class of Hamiltonians exhibits rich phase diagrams and relates to

quantum magnetism, high-temperature superconductors, and magnetic insulators, among many other applications.^{35–37} Our approach is distinct from those of existing experimental demonstrations and theoretical proposals for the simulation of such Hamiltonians,³⁸ which include ultracold atoms on optical lattices,^{39–41} trapped ions,⁴² and superconducting qubits.^{43–49} We note that our approach is distinct from previous realizations of photonic mesh lattices using two-loop architectures,^{50–53} which implement a discrete-time non-interacting quantum walk that is limited in the number of evolution steps due to the ratio between the pulse period and the difference in round-trip times. In contrast, our setup implements a Trotterized version of a continuous-time interacting quantum walk. Moreover, our scheme can create arbitrarily shaped lattices in higher dimensions through active modulation control, whereas the two-loop architectures need physical modifications to increase dimensionality or change the connectivity of the lattice.

We propose a system that emulates the dynamics of the Hamiltonian in Eq. (1) using a synthetic temporal dimension. The design

consists of a waveguide loop exhibiting Kerr nonlinearity, the “storage ring,” in which a train of single-photon pulses propagates in a single direction, with each pulse occupying its own time bin. A second loop, the “register,” is connected to the storage ring using a Mach-Zehnder interferometer (MZI) with two tunable phase shifters, θ and ϕ . The hardware of the device is chosen to emulate each term of the Hamiltonian with dedicated components. The first term of Eq. (1) is implemented by the tunable MZI; the second term arises naturally from the total photon energy in each time bin; and the two-photon potential in the third term results from using a Kerr-nonlinear fiber for the storage and register loops. We will briefly derive how each component implements the desired behavior and then describe how to program the device.

A system evolving for a time interval t under the Hamiltonian given in Eq. (1) has a propagator $e^{-i\hat{H}t}$. We can split the exponential of the summation into a product of exponentials to within $\mathcal{O}(\kappa^2 t^2 + \kappa U t^2 \cos \alpha)$, where κ and α are typical values of κ_{mn}, α_{mn} (see the supplementary material for a more detailed derivation),

$$e^{-i\hat{H}t} = \exp \left[-it \left(- \sum_{\langle m,n \rangle} \kappa_{mn} (e^{i\alpha_{mn}} \hat{a}_m^\dagger \hat{a}_m + e^{-i\alpha_{mn}} \hat{a}_n^\dagger \hat{a}_m) + \mu \sum_m \hat{a}_m^\dagger \hat{a}_m + U \sum_m \hat{a}_m^\dagger \hat{a}_m^\dagger \hat{a}_m \hat{a}_m \right) \right] \\ \approx \left[\prod_{\langle m,n \rangle} \exp \left(i\kappa_{mn} (e^{i\alpha_{mn}} \hat{a}_m^\dagger \hat{a}_m + e^{-i\alpha_{mn}} \hat{a}_n^\dagger \hat{a}_m) \right) \right]^t \times e^{-it \left(\mu \sum_m \hat{a}_m^\dagger \hat{a}_m + U \sum_m \hat{a}_m^\dagger \hat{a}_m^\dagger \hat{a}_m \hat{a}_m \right)}. \quad (2)$$

We, therefore, have a propagator that is a product of two parts: a continuous time evolution term $e^{-it(\mu \sum_m \hat{a}_m^\dagger \hat{a}_m + U \sum_m \hat{a}_m^\dagger \hat{a}_m^\dagger \hat{a}_m \hat{a}_m)}$, which arises naturally from the photon energy per time bin (μ) and Kerr nonlinearity of the fiber (U), and the $\exp(i\kappa_{mn} e^{i\alpha_{mn}} \hat{a}_m^\dagger \hat{a}_m + \text{H.c.})$ terms, which are implemented in discrete time evolution by a sequence of passes through the tunable MZI. We now show how the device physics emulates the dynamics of the propagator.

For the chemical potential term, we can write the Hamiltonian for a photon with an arbitrary spectrum as $\hat{H}_{\text{EM}} = \int dk \sum_m \frac{1}{2} \hbar \omega_k (\hat{a}_{m,k}^\dagger \hat{a}_{m,k} + \hat{a}_{m,k} \hat{a}_{m,k}^\dagger)$. If we can assume that the photons are spectrally narrow about a carrier frequency ω_0 , we can approximate this as $\hat{H}_{\text{EM}} \approx \frac{1}{2} \hbar \omega_0 \sum_m (\hat{a}_m^\dagger \hat{a}_m + \hat{a}_m \hat{a}_m^\dagger) = \hbar \omega_0 \sum_m (\hat{a}_m^\dagger \hat{a}_m + \frac{1}{2}) \equiv \mu \sum_m \hat{a}_m^\dagger \hat{a}_m$, which directly gives us the desired chemical potential term.

The nonlinear potential naturally arises from the use of a nonlinear fiber. Consider a section of a Kerr-nonlinear fiber corresponding to one time bin, with length Δx and volume V . The material polarization at frequency ω induced by an electric field $E(\omega)$ is given by $\mathcal{P}_{\text{NL}}(\omega) = 3\epsilon_0 \chi^{(3)}(\omega) |E(\omega)|^2 E(\omega)$, where $\chi^{(3)}$ is the third-order susceptibility tensor, which, for simplicity, we treat as a scalar. The energy density \mathcal{U}_{NL} is related as $\mathcal{P}_{\text{NL}} = \partial \mathcal{U}_{\text{NL}} / \partial E^*$, and the Hamiltonian of this system, again assuming a narrow bandwidth about ω_0 , is $\hat{H}_{\text{NL}} = \int_V \mathcal{U}_{\text{NL}}(\omega_0) d^3 \vec{r}$. After quantizing the field amplitudes as $E(\omega_0) \mapsto \sqrt{\frac{\hbar \omega_0}{2\epsilon_0 V}} (\hat{a}_{k_0}^\dagger e^{+i(\omega_0 t - k_0 z)} + \text{H.c.})$ and transforming into real space, we obtain $\hat{H}_{\text{NL}} = \left(\frac{9\hbar^2 \omega_0^2}{8\epsilon_0 n_0^4 V^2} \int_V \chi^{(3)} d^3 \mathbf{r} \right) \hat{a}^\dagger \hat{a}^\dagger \hat{a} \hat{a} + C$

$\equiv U \hat{a}^\dagger \hat{a}^\dagger \hat{a} \hat{a} + C$, where the nonlinear potential coefficient is $U = \frac{9\hbar^2 \omega_0^2}{8\epsilon_0 n_0^4 V^2} \int_V \chi^{(3)} d^3 \mathbf{r}$ and where C is some constant corresponding to an overall energy shift. Applying this to each time bin gives us the desired $U \sum_m \hat{a}_m^\dagger \hat{a}_m^\dagger \hat{a}_m \hat{a}_m$ nonlinear potential term. Note that this interaction term U and its estimation from the material nonlinearity $\chi^{(3)}$ is subject to the usual caveats that have been discussed in the literature when the U is large; however, we may be able to circumvent these issues partially since the nonlinear phase shift per clock cycle can be designed to be small while still achieving a large U/κ .^{54–56}

Finally, the hopping terms arise from programmatically modulating the phase shifts in the MZI. To interfere two photons m and n with strength κ_{mn} and phase shift α_{mn} , the basic idea is to swap pulse m into the register ring, wait for pulse n to reach the MZI, interfere the pulses, and then return pulse m to the storage ring when time bin m cycles back. The following calculations are done in greater detail in Sec. I of the supplementary material. Consider the MZI shown in Fig. 1(a) with phase shifters $\pm\phi$ and θ . Define bosonic mode operators $\hat{a}_n^\dagger, \hat{a}_0^\dagger$ and $\hat{b}_n^\dagger, \hat{b}_0^\dagger$, which create a photon in time bin n or time bin 0 (the register bin) and at the input or output of the MZI, respectively. We can relate the output and input mode operators as

$$\begin{bmatrix} \hat{b}_0^\dagger \\ \hat{b}_n^\dagger \end{bmatrix} = e^{-i\frac{\theta}{2} (e^{i\phi} \hat{a}_0^\dagger \hat{a}_n + \text{H.c.})} \begin{bmatrix} \hat{a}_0^\dagger \\ \hat{a}_n^\dagger \end{bmatrix} \equiv \hat{M}_{0,n}(\theta, \phi) \begin{bmatrix} \hat{a}_0^\dagger \\ \hat{a}_n^\dagger \end{bmatrix}. \quad (3)$$

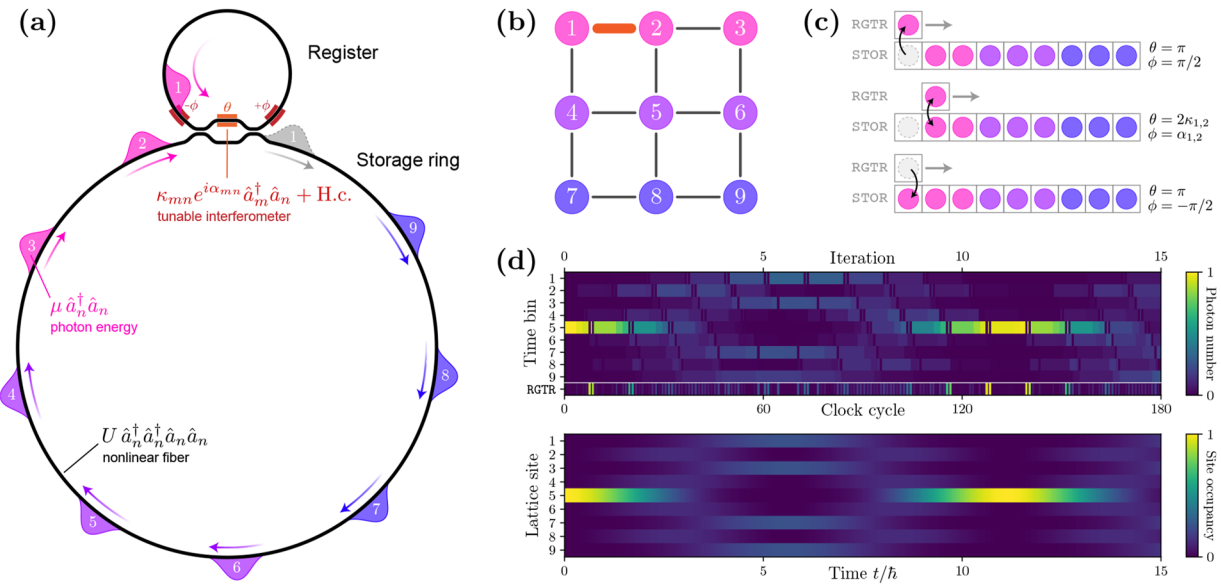


FIG. 1. Architecture for the programmable photonic quantum emulator. (a) The physical design of the device. Classical laser pulses or single-photon pulses propagate through a fiber storage ring. A programmable Mach–Zehnder interferometer connects the storage ring to a register loop, which has an optical path length Δx equal to the length of a single time bin. By setting the phase shift values in the MZI, the hopping coefficients and phases (κ_{mn}, α_{mn}) can be programmatically adjusted. Photons have energy $\mu \equiv \hbar\omega_0$, and by using a $\chi^{(3)}$ -nonlinear fiber, a nonlinear interaction potential U can be applied. (b) An example 2D grid lattice to be emulated by the device. Node labels correspond to photon pulse indices, and the device as depicted in panel (a) is constructing the orange edge connecting nodes 1 and 2 with (κ_{12}, α_{12}). (c) Illustration of a single clock cycle (defined as the round-trip time through the storage ring) of the emulator applying the interaction (κ_{12}, α_{12}) in three steps, shown as the three rows. The colors of the time bins match the node colors in panel (b) for visual clarity, with θ and ϕ labels denoting MZI phase shifts per step. First, phase shifters are set to transfer photon 1 into the register, where it circulates for one path length (equal to 1/9 the path length of the storage ring, depicted in the figure by the register bin moving to the right by one bin relative to storage). Second, photon 1 is interacted with photon 2 using $\theta = 2\kappa_{12}$ and $\phi = \alpha_{12}$. Third, the pulse (which now contains a mixture of photons 1 and 2) is returned to its original time bin after propagating through the register ring eight more times. (d) The evolution of the state of the device while emulating a tight-binding Hamiltonian over the lattice shown in panel (b). The bottom panel depicts the exact evolution of $e^{-iHt/\hbar}$ over a wall-clock time t/\hbar , while the top panel shows the state of the emulator at each clock cycle, including register swaps (depicted as the dark/light bands in the storage/register rows) and intermediate states between full iterations. A large value of $\kappa = 0.2$ was used for visual clarity, but more accurate results may be obtained by using smaller κ and running the emulation for a commensurately longer wall-clock time.

It is easily verified that the following identity holds: $\hat{M}_{0,m}(\pi, -\pi/2) \hat{M}_{0,n}(\theta, \phi) \hat{M}_{0,m}(\pi, +\pi/2) = \exp[-i\theta/2(e^{i\phi} \hat{a}_m^\dagger \hat{a}_n + e^{-i\phi} \hat{a}_n^\dagger \hat{a}_m)] \equiv \hat{T}_{m,n}(\theta, \phi)$. If we define $\kappa \equiv -\theta/2$ and $\alpha \equiv +\phi$, we obtain the transfer matrix as

$$\hat{T}_{mn}(\kappa, \alpha) = \exp[i\kappa(e^{i\alpha} \hat{a}_m^\dagger \hat{a}_n + e^{-i\alpha} \hat{a}_n^\dagger \hat{a}_m)]. \quad (4)$$

The middle θ phase shifter thus allows us to control the strength of the coupling κ , while the outer phase shifters $\pm\phi$ control the hopping phases α . (Note that the effects of $\pm\phi$ cancel while the photon is circulating in the register ring, but they do not cancel on entry/exit from the register, keeping the register and storage phases aligned.)

By performing this sequence of passes through the MZI $\hat{T}_{\langle m,n \rangle} \equiv \prod_{\langle m,n \rangle} \hat{T}_{mn}(\kappa_{mn}, \alpha_{mn})$ for every photon pair $\langle m, n \rangle$, which corresponds to an interacting pair of lattice sites m and n in the Hamiltonian, we complete one “iteration” of the emulator. The lattice sites can be interacted in any order as long as the values of κ are small (see the supplementary material, Secs. I and IA), which is always possible to do by decreasing κ , μ , and U by some constant factor and running the emulator for a commensurately longer wall-clock time. If we allow the system to evolve for t iterations, we obtain a total transfer matrix, which is exactly the first term in Eq. (2),

$$\hat{T}_{\langle m,n \rangle}^t = \left(\prod_{\langle m,n \rangle} \exp[i\kappa_{mn}(e^{i\alpha_{mn}} \hat{a}_m^\dagger \hat{a}_n + \text{H.c.})] \right)^t. \quad (5)$$

Therefore, all three components of the propagator are present, and the evolution of a state in the device for t iterations is described term-by-term by the propagator in Eq. (2). To adjust the relative values of continuous time evolution variables (μ, U) and discrete time evolution variables (κ, α), one can adjust the photon energies μ , Kerr interaction strength U , time bin size Δx , or phase shifter values θ, ϕ , potentially circumventing the issues raised in Ref. 54.

To provide some realistic experimental parameters, the 2D grid lattice in Fig. 1(b) can be emulated using a register ring with a fiber length of 20 cm and a storage ring with a fiber length of 1.8 m to accommodate nine time bins of 1 ns. Since there are 18 interactions to construct, the total operation time would be 162 ns (18 clock cycles). The minimum duration of a time bin is limited by the switching speed of the phase shifters, which can range from 10 to 50 GHz in lithium niobate and barium titanate platforms.^{57,58} Further discussion of experimental details can be found in the supplementary material.

To more concretely show the capabilities of our proposed device, we now provide several demonstrations of the device emulating interesting systems with experimentally measurable signatures. We show the device can create an effective gauge potential by emulating a synthetic Hall ladder, we demonstrate the quantum nature of the device by trapping a two-photon state using a synthetic field, and we demonstrate the reconfigurability of the device by emulating the evolution of a Bose–Hubbard Hamiltonian on a four-dimensional tesseract lattice. For these demonstrations, we wrote a Python simulator built with QuTiP⁵⁹ to tractably simulate the system using a permutationally invariant bosonic lattice representation of the system state space. This simulation method is described in greater detail in the supplementary material and is available online at github.com/fancompute/synthetic-hamiltonians.

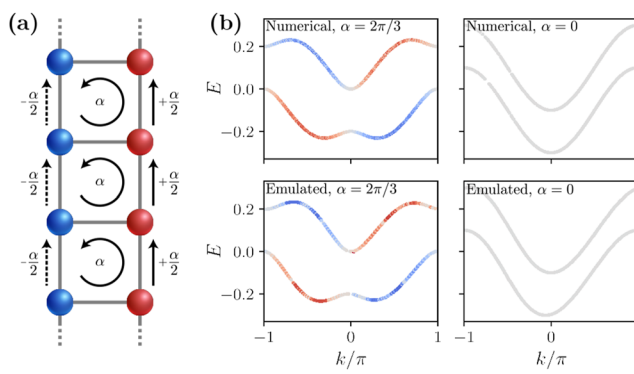


Figure 2 shows an emulated synthetic Hall ladder and obtains a similar band structure as the recent experimental results of Ref. 1. The actual physics of the emulation device are simulated to derive this result. The system is evolved for 200 iterations; using the naive interaction method described in Fig. 1(c), this would take a wall-clock time of 32 ms, but a more sophisticated scheme presented in Sec. VI of the supplementary material can parallelize the emulation of this lattice to reduce this time by three orders of magnitude to 40 μ s.

The system shown in Fig. 2 exhibits chiral edge states in the presence of an effective magnetic field, which is induced by adding translation-invariant hopping phases $\pm\alpha/2$ to the outer edges of the ladder using the MZI. **Figure 2(a)** depicts the emulated ladder system; left and right nodes on each rung are mapped to pulses in even-

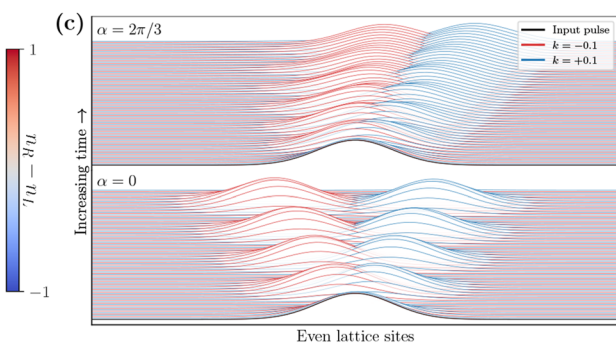


FIG. 2. (a) Lattice diagram for a two-legged synthetic Hall ladder emulated with the device. (b) Band structure of the system computed by diagonalizing the Hamiltonian for the exact case (top row) or the matrix logarithm of the propagator for the emulated case (bottom row) in the presence (left) and absence (right) of a synthetic magnetic field. Color denotes photon occupancy on the left and right sides of the ladder. (c) Propagation of chiral edge currents on the left leg of the ladder. A Gaussian input state is created with some initial $k = \pm 0.1$ by exciting multiple time bins corresponding to the nodes of the left leg of the ladder with a phase difference between bins. When the gauge field is turned on ($\alpha = 2\pi/3$), the motion in one direction is inhibited.

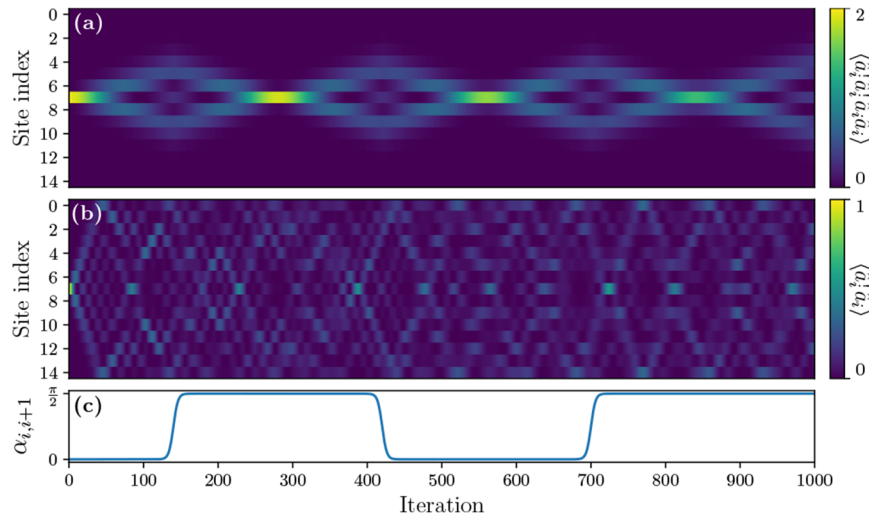


FIG. 3. Emulated evolution of (a) a two-photon state and (b) a single-photon state in a 1D lattice as (c) time-dependent hopping phases are varied. The changing hopping phases introduce a changing gauge potential that causes the two-photon state to experience an effective electric field. The single-photon state is unaffected by this field. Parameters used in the simulated device: $\kappa = 0.1$ and $U = 0.8$.

and odd-indexed time bins. The band structures for the target and emulated Hamiltonians for this system are shown in Fig. 2(b) for hopping phases $\alpha = 2\pi/3$ and $\alpha = 0$. (The band structures for the synthetic case are computed by simulating one iteration of the propagator $\hat{G} = e^{-i\hat{H}(t=1)}$ in the device, taking the matrix logarithm $\hat{H} = \frac{\log \hat{G}}{-i}$, and then diagonalizing \hat{H} ; k values are computed using peak detection of the eigenstate Fourier transform; see the supplementary material for more detail.) The band structures from the emulated system (bottom row) closely match the desired band structures (top row; see also Ref. 60), as well as the experimental results from very different platforms (Fig. 2 of Ref. 1). This shows that the simulation of our device physics faithfully constructs the desired synthetic Hall Hamiltonian. Chiral edge states are clearly visible in the case of $\alpha = 2\pi/3$, indicating the presence of an effective gauge potential. The propagation of these chiral currents on the left leg of the ladder is shown Fig. 2(c). In the presence of a gauge field, only one-way motion is permitted.

Next, to demonstrate the quantum capabilities of the device, we show how a two-photon state can be manipulated by introducing time-dependent hopping phases $\alpha(t)$ on a 1D lattice while using nonlinearity, which is strong compared to the coupling constants $U \gg \kappa$. Figure 3 depicts the evolution of a two-photon state and a single-photon state under time-dependent hopping phases $\alpha(t)$. The energetic gap between $U \gg \kappa$ means that while $\alpha(t) = 0$, the two-photon state evolves the same as the single-photon state but with a slower timescale for the evolution. [The two-photon state in panel (a) undergoes slower evolution because the Hamiltonian has no terms that can transport two photons simultaneously between lattice sites. Thus, evolution is allowed only via single-photon transport through an intermediate state that is lower in energy by U , which never develops a sizable population because it is off-resonant from the initial and final states.] As $\alpha(t)$ is changed, $\partial\alpha/\partial t$ introduces an effective field, analogous to $\vec{E} = -\nabla V - \partial\vec{A}/\partial t$, which causes the two-photon state to look like it is “lensing” back to its original configuration. This field is maximized at odd multiples of $\pi/2$, and by choosing suitable amplitude, duration, and periodicity of $\alpha(t)$, the two-photon state can effectively be trapped in the center of the lattice. The single-photon state is unaffected by the field, since we can perform a gauge transformation of the single-photon basis states as $\hat{a}_n^\dagger \mapsto \hat{b}_n^\dagger e^{i\alpha_n(t)}$, which eliminates the effect of $\alpha(t)$. Note that this two-photon trapping behavior can be related to the

photon bound states that have been extensively studied in waveguide quantum electrodynamics (QED) and cavity QED.^{61–67} Assuming a 100 ps pulse with an effective mode area of $1 \mu\text{m}^2$, our simulated U value corresponds to a $\chi^{(3)}$ nonlinearity of $\approx 2.84 \times 10^{-14} \text{ m}^2/\text{V}^2$. Such a value is achievable using photonic crystal fibers filled with high-density atomic gas, which can have a $\chi^{(3)}$ nonlinearity of $\approx 5.3 \times 10^{-12} \text{ m}^2/\text{V}^2$.^{68,69}

Finally, we demonstrate how the programmable nature of the device allows for emulation of complex, high-dimensional topologies. Figure 4 shows the evolution of a tight-binding Hamiltonian over a four-dimensional tesseract lattice emulated using the device. This demonstration uses a single degree of freedom (time) to emulate four independent physical synthetic dimensions. A projection of the non-planar graph defining the lattice is shown in Fig. 4(a). The evolution of a state with two bosons (emulated by classical laser pulses) in this tesseract lattice is shown in Fig. 4(b); bosons are initially placed in time bins 0 and 5, and oscillations across the tesseract are visible, with the bosons oscillating between sites 0 \leftrightarrow 10 and 5 \leftrightarrow 15. (This is the expected behavior, representing the four-dimensional analog of a boson oscillating between the corners of a 2×2 square lattice.) Two-photon correlation matrices are shown at different points in time in the upper panels. The state is plotted at the end of each iteration of the device; since photons have been swapped out of register time bin at the end of each iteration, it is shown to be empty at all times.

The simplicity of the design of the device and the flexibility it provides make it appealing from an experimental perspective. A detailed error analysis of this design in the presence of experimental imperfections is presented in the supplementary material, which we summarize here. Dispersion within the fiber loops is not a concern until photons travel a total path length of thousands of kilometers. Optical attenuation in the fiber is not an issue for classically emulable cases (where the total boson number is $N = 1$ or where the initial state is well-approximated by a coherent state) such as the Hall ladder in Fig. 2, since pulses can be re-amplified as needed. Quantum emulations require single photon pulses that cannot be re-amplified, but commercially available fibers have sufficiently low attenuation to allow for emulation of small lattice systems with very high fidelities per iteration. Finally, sufficiently high values of the nonlinear potential U have been demonstrated using crystal fibers with high-density atomic gas,^{68,69} and integrated photonic platforms^{70,71} (albeit

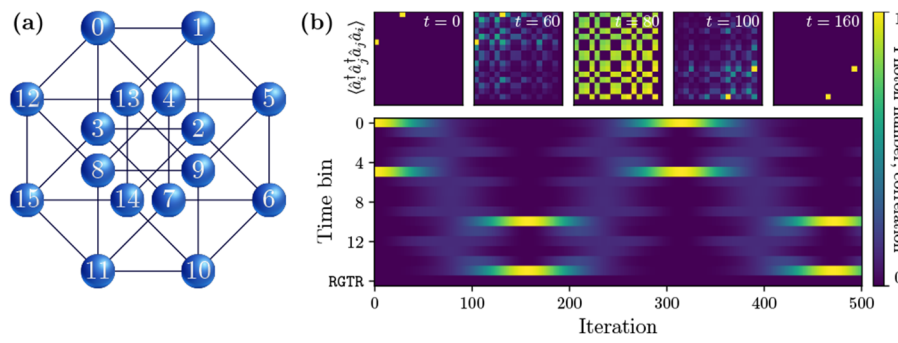


FIG. 4. Emulation of a tight-binding Hamiltonian over a four-dimensional tesseract. (a) Projection of the tesseract graph that defines the lattice. (b) Evolution of a tesseract lattice containing two emulated bosons exhibiting oscillations between time bins $0 \leftrightarrow 10$ and $5 \leftrightarrow 15$. Parameters: $\kappa = 0.01$, $\alpha = \mu = U = 0$.

in $\chi^{(2)}$ materials) show promise for achieving even higher values of U in the near future.

In summary, we have presented a theoretical design for a programmable photonic device capable of emulating a broad class of classical and quantum Hamiltonians in lattices with arbitrary topologies. The device contains only a single actively controlled optical component—a phase-modulated MZI—and can be reprogrammed to emulate a wide variety of systems, such as chiral states in a Hall ladder, synthetic gauge potentials, and high-dimensional lattices. Our proposed device is an experimentally appealing platform that opens up new possibilities for studying fundamental topological and many-body physics.

SUPPLEMENTARY MATERIAL

The supplementary material includes derivations of the correspondence between the device physics and the Hamiltonian, details on the numerical simulations and experimental implementation, and the optimized emulation schemes for larger lattices.

ACKNOWLEDGMENTS

This work was supported by a Vannevar Bush Faculty Fellowship from the U.S. Department of Defense (Grant No. N00014-17-1-3030) and by an AFOSR MURI project (Grant No. FA9550-22-1-0339). A.D. was partially supported by a National Quantum Lab at Maryland (Q-Lab) seed grant.

AUTHOR DECLARATIONS

Conflict of Interest

The authors have no conflicts to disclose.

Author Contributions

Ben Bartlett: Conceptualization (equal); Data curation (lead); Formal analysis (lead); Investigation (lead); Methodology (lead); Software (lead); Visualization (lead); Writing – original draft (lead); Writing – review & editing (equal). **Olivia Y. Long:** Investigation (supporting); Methodology (supporting); Validation (supporting); Writing – review & editing (supporting). **Avik Dutt:** Conceptualization (equal); Investigation (supporting); Methodology (equal); Validation (supporting); Writing – review & editing (equal). **Shanhui Fan:** Conceptualization (equal); Funding acquisition (lead); Project administration (lead); Resources (lead); Supervision (lead); Writing – review & editing (equal).

DATA AVAILABILITY

The data that support the findings of this study are openly available in github.com/fancompute/synthetic-hamiltonians.

REFERENCES

- ¹A. Dutt, Q. Lin, L. Yuan, M. Minkov, M. Xiao, and S. Fan, “A single photonic cavity with two independent physical synthetic dimensions,” *Science* **367**, 59–64 (2020).
- ²L. Yuan, Q. Lin, M. Xiao, and S. Fan, “Synthetic dimension in photonics,” *Optica* **5**, 1396–1405 (2018).
- ³Y. Baum and G. Refael, “Setting boundaries with memory: Generation of topological boundary states in Floquet-induced synthetic crystals,” *Phys. Rev. Lett.* **120**, 106402 (2018).
- ⁴H. Price, Y. Chong, A. Khanikaev, H. Schomerus, L. J. Maczewsky, M. Kremer, M. Heinrich, A. Szameit, O. Zilberman, Y. Yang, B. Zhang, A. Alu, R. Thomale, I. Carusotto, P. St-Jean, A. Amo, A. Dutt, L. Yuan, S. Fan, X. Yin, C. Peng, T. Ozawa, and A. Blanco-Redondo, “Roadmap on topological photonics,” *J. Phys.: Photonics* **4**, 032501 (2022).
- ⁵T. Ozawa and H. M. Price, “Topological quantum matter in synthetic dimensions,” *Nat. Rev. Phys.* **1**, 349–357 (2019).
- ⁶T. Inagaki, Y. Haribara, K. Igarashi, T. Sonobe, S. Tamate, T. Honjo, A. Marandi, P. L. McMahon, T. Umeki, K. Enbusu, O. Tadanaga, H. Takenouchi, K. Aihara, K.-i. Kawarabayashi, K. Inoue, S. Utsunomiya, and H. Takesue, “A coherent Ising machine for 2000-node optimization problems,” *Science* **354**, 603–606 (2016).
- ⁷P. L. McMahon, A. Marandi, Y. Haribara, R. Hamerly, C. Langrock, S. Tamate, T. Inagaki, H. Takesue, S. Utsunomiya, K. Aihara, R. L. Byer, M. M. Fejer, H. Mabuchi, and Y. Yamamoto, “A fully programmable 100-spin coherent Ising machine with all-to-all connections,” *Science* **354**, 614–617 (2016).
- ⁸A. Marandi, Z. Wang, K. Takata, R. L. Byer, and Y. Yamamoto, “Network of time-multiplexed optical parametric oscillators as a coherent Ising machine,” *Nat. Photonics* **8**, 937–942 (2014).
- ⁹B. Peng, S. Yan, D. Cheng, D. Yu, Z. Liu, V. Y. Vladislav, L. Yuan, and X. Chen, “Optical neural network architecture for deep learning with temporal synthetic dimension,” *Chinese Phys. Lett.* **40**, 034201 (2023); <https://iopscience.iop.org/article/10.1088/0256-307X/40/3/034201>.
- ¹⁰O. Boada, A. Celi, J. I. Latorre, and M. Lewenstein, “Quantum simulation of an extra dimension,” *Phys. Rev. Lett.* **108**, 133001 (2012).
- ¹¹T. Ozawa, H. M. Price *et al.*, “Synthetic dimensions in integrated photonics: From optical isolation to four-dimensional quantum Hall physics,” *Phys. Rev. A* **93**, 043827 (2016).
- ¹²H. Chalabi, S. Barik, S. Mittal, T. E. Murphy, M. Hafezi, and E. Waks, “Synthetic gauge field for two-dimensional time-multiplexed quantum random walks,” *Phys. Rev. Lett.* **123**, 150503 (2019).
- ¹³B. Bartlett, A. Dutt, and S. Fan, “Deterministic photonic quantum computation in a synthetic time dimension,” *Optica* **8**, 1515 (2021).
- ¹⁴M. Pysher, Y. Miwa, R. Shahrokhsahi, R. Bloomer, and O. Pfister, “Parallel generation of quadrupartite cluster entanglement in the optical frequency comb,” *Phys. Rev. Lett.* **107**, 030505 (2011).
- ¹⁵J. Roslund, R. M. de Araújo, S. Jiang, C. Fabre, and N. Treps, “Wavelength-multiplexed quantum networks with ultrafast frequency combs,” *Nat. Photonics* **8**, 109–112 (2014).
- ¹⁶J. Yoshikawa, S. Yokoyama, T. Kaji, C. Sornphiphatphong, Y. Shiozawa, K. Makino, and A. Furusawa, “Invited article: Generation of one-million-mode continuous-variable cluster state by unlimited time-domain multiplexing,” *APL Photonics* **1**, 060801 (2016).
- ¹⁷M. V. Larsen, X. Guo, C. R. Breum, J. S. Neergaard-Nielsen, and U. L. Andersen, “Deterministic generation of a two-dimensional cluster state,” *Science* **366**, 369–372 (2019).
- ¹⁸E. Lustig, S. Weimann, Y. Plotnik, Y. Lumer, M. A. Bandres, A. Szameit, and M. Segev, “Photonic topological insulator in synthetic dimensions,” *Nature* **567**, 356–360 (2019).
- ¹⁹A. Regensburger, C. Bersch, M.-A. Miri, G. Onishchukov, D. N. Christodoulides, and U. Peschel, “Parity-time synthetic photonic lattices,” *Nature* **488**, 167–171 (2012).
- ²⁰M. Wimmer, H. M. Price, I. Carusotto, and U. Peschel, “Experimental measurement of the Berry curvature from anomalous transport,” *Nat. Phys.* **13**, 545–550 (2017).
- ²¹C. Leefmans, A. Dutt, J. Williams, L. Yuan, M. Parto, F. Nori, S. Fan, and A. Marandi, “Topological dissipation in a time-multiplexed photonic resonator network,” *Nat. Phys.* **18**, 442 (2022).
- ²²K. Tiurev, P. L. Mirambell, M. B. Lauritzen, M. H. Appel, A. Tiranov, P. Lodahl, and A. S. Sørensen, “Fidelity of time-bin-entangled multiphoton states from a quantum emitter,” *Phys. Rev. A* **104**, 052604 (2021).
- ²³P. Hilaire, L. Vidro, H. S. Eisenberg, and S. E. Economou, “Near-deterministic hybrid generation of arbitrary photonic graph states using a single quantum emitter and linear optics,” *Quantum* **7**, 992 (2023).

- ²⁴L. Yuan, Y. Shi, and S. Fan, "Photonic gauge potential in a system with a synthetic frequency dimension," *Opt. Lett.* **41**, 741–744 (2016).
- ²⁵B. A. Bell, K. Wang, A. S. Solntsev, D. N. Neshev, A. A. Sukhorukov, and B. J. Eggleton, "Spectral photonic lattices with complex long-range coupling," *Optica* **4**, 1433–1436 (2017).
- ²⁶Y. Hu, C. Reimer, A. Shams-Ansari, M. Zhang, and M. Loncar, "Realization of high-dimensional frequency crystals in electro-optic microcombs," *Optica* **7**, 1189–1194 (2020).
- ²⁷K. Wang, B. A. Bell, A. S. Solntsev, D. N. Neshev, B. J. Eggleton, and A. A. Sukhorukov, "Multidimensional synthetic chiral-tube lattices via nonlinear frequency conversion," *Light: Sci. Appl.* **9**, 132 (2020).
- ²⁸A. Celi, P. Massignan, J. Ruseckas, N. Goldman, I. B. Spielman, G. Juzeliunas, and M. Lewenstein, "Synthetic gauge fields in synthetic dimensions," *Phys. Rev. Lett.* **112**, 043001 (2014).
- ²⁹M. Mancini, G. Pagano, G. Cappellini, L. Livi, M. Rider, J. Catani, C. Sias, P. Zoller, M. Inguscio, M. Dalmonte, and L. Fallani, "Observation of chiral edge states with neutral fermions in synthetic Hall ribbons," *Science* **349**, 1510–1513 (2015).
- ³⁰B. K. Stuhl, H.-I. Lu, L. M. Aycock, D. Genkina, and I. B. Spielman, "Visualizing edge states with an atomic Bose gas in the quantum Hall regime," *Science* **349**, 1514–1518 (2015).
- ³¹X.-W. Luo, X. Zhou, C.-F. Li, J.-S. Xu *et al.*, "Quantum simulation of 2D topological physics in a 1D array of optical cavities," *Nat. Commun.* **6**, 7704 (2015).
- ³²L. Yuan, Q. Lin, A. Zhang, M. Xiao, X. Chen, and S. Fan, "Photonic gauge potential in one cavity with synthetic frequency and orbital angular momentum dimensions," *Phys. Rev. Lett.* **122**, 083903 (2019).
- ³³O. Dutta, M. Gajda, P. Hauke, M. Lewenstein, D.-S. Luhmann, B. A. Malomed, T. Sowinski, and J. Zakrzewski, "Non-standard Hubbard models in optical lattices: A review," *Rep. Prog. Phys.* **78**, 066001 (2015).
- ³⁴C. Repellin, J. Léonard, and N. Goldman, "Fractional Chern insulators of few bosons in a box: Hall plateaus from center-of-mass drifts and density profiles," *Phys. Rev. A* **102**, 063316 (2020).
- ³⁵A. Auerbach, *Interacting Electrons and Quantum Magnetism*, 1st ed. (Springer-Verlag, New York, 1994).
- ³⁶V. Zapf, M. Jaime, and C. D. Batista, "Bose-Einstein condensation in quantum magnets," *Rev. Mod. Phys.* **86**, 563–614 (2014).
- ³⁷T. Giamarchi, C. Rüegg, and O. Tchernyshyov, "Bose-Einstein condensation in magnetic insulators," *Nat. Phys.* **4**, 198–204 (2008).
- ³⁸E. Altman, K. R. Brown, G. Carleo, L. D. Carr, E. Demler, C. Chin, B. DeMarco, S. E. Economou, M. A. Eriksson, K.-M. C. Fu, M. Greiner, K. R. A. Hazzard, R. G. Hulet, A. J. Kollár, B. L. Lev, M. D. Lukin, R. Ma, X. Mi, S. Misra, C. Monroe, K. Murch, Z. Nazario, K.-K. Ni, A. C. Potter, P. Roushan, M. Saffman, M. Schleier-Smith, I. Siddiqi, R. Simmonds, M. Singh, I. B. Spielman, K. Temme, D. S. Weiss, J. Vučković, V. Vuletić, J. Ye, and M. Zwierlein, "Quantum simulators: Architectures and opportunities," *PRX Quantum* **2**(1), 017003 (2021).
- ³⁹M. Hafezi, A. S. Sørensen, E. Demler, and M. D. Lukin, "Fractional quantum Hall effect in optical lattices," *Phys. Rev. A* **76**, 023613 (2007).
- ⁴⁰B. Yang, H. Sun, R. Ott, H.-Y. Wang, T. V. Zache, J. C. Halimeh, Z.-S. Yuan, P. Hauke, and J.-W. Pan, "Observation of gauge invariance in a 71-site Bose-Hubbard quantum simulator," *Nature* **587**, 392–396 (2020).
- ⁴¹A. González-Tudela, C.-L. Hung, D. E. Chang, J. I. Cirac, and H. J. Kimble, "Subwavelength vacuum lattices and atom-atom interactions in two-dimensional photonic crystals," *Nat. Photonics* **9**, 320–325 (2015).
- ⁴²R. Blatt and C. F. Roos, "Quantum simulations with trapped ions," *Nat. Phys.* **8**, 277–284 (2012).
- ⁴³G. P. Fedorov, S. V. Remizov, D. S. Shapiro, W. V. Pogosov, E. Egorova, I. Tsitsilin, M. Andronik, A. A. Dobronosova, I. A. Rodionov, O. V. Astafiev, and A. V. Ustinov, "Photon transport in a Bose-Hubbard chain of superconducting artificial atoms," *Phys. Rev. Lett.* **126**, 180503 (2021).
- ⁴⁴R. Ma, B. Saxberg, C. Owens, N. Leung, Y. Lu, J. Simon, and D. I. Schuster, "A dissipatively stabilized Mott insulator of photons," *Nature* **566**(7742), 51–57 (2019).
- ⁴⁵L. W. Clark, N. Jia, N. Schine, C. Baum, A. Georgakopoulos, and J. Simon, "Interacting Floquet polaritons," *Nature* **571**(7766), 532–536 (2019).
- ⁴⁶L. W. Clark, N. Schine, C. Baum, N. Jia, and J. Simon, "Observation of Laughlin states made of light," *Nature* **582**(7810), 41–45 (2020).
- ⁴⁷P. Roushan, C. Neill, A. Megrant, Y. Chen, R. Babbush, R. Barends, B. Campbell, Z. Chen, B. Chiaro, A. Dunsworth, A. Fowler, E. Jeffrey, J. Kelly, E. Lucero, J. Mutus, P. J. J. O'Malley, M. Neeley, C. Quintana, D. Sank, A. Vainsencher, J. Wenner, T. White, E. Kapit, H. Neven, and J. Martinis, "Chiral ground-state currents of interacting photons in a synthetic magnetic field," *Nat. Phys.* **13**(2), 146–151 (2017).
- ⁴⁸P. Roushan, C. Neill, J. Tangpanitanon, V. M. Bastidas, A. Megrant, R. Barends, Y. Chen, Z. Chen, B. Chiaro, A. Dunsworth, A. Fowler, B. Foxen, M. Giustina, E. Jeffrey, J. Kelly, E. Lucero, J. Mutus, M. Neeley, C. Quintana, D. Sank, A. Vainsencher, J. Wenner, T. White, H. Neven, D. G. Angelakis, and J. Martinis, "Spectroscopic signatures of localization with interacting photons in superconducting qubits," *Science* **358**(6367), 1175–1179 (2017).
- ⁴⁹A. Rahmani, K. J. Sung, H. Puttermann, P. Roushan, P. Ghaemi, and Z. Jiang, "Creating and manipulating a Laughlin-type $\nu = 1/3$ fractional quantum Hall state on a quantum computer with linear depth circuits," *PRX Quantum* **1**(2), 020309 (2020).
- ⁵⁰A. Schreiber, A. Gábris, P. P. Rohde, K. Laiho, M. Štefaňák, V. Potoček, C. Hamilton, I. Jex, and C. Silberhorn, "A 2D quantum walk simulation of two-particle dynamics," *Science* **336**(6077), 55–58 (2012).
- ⁵¹A. L. M. Muniz, M. Wimmer, A. Bisianov, U. Peschel, R. Morandotti, P. S. Jung, and D. N. Christodoulides, "2D solitons in \mathcal{PT} -symmetric photonic lattices," *Phys. Rev. Lett.* **123**(25), 253903 (2019).
- ⁵²A. L. M. Muniz, M. Wimmer, A. Bisianov, R. Morandotti, and U. Peschel, "Collapse on the line—How synthetic dimensions influence nonlinear effects," *Sci. Rep.* **9**(1), 9518 (2019).
- ⁵³M. Wimmer, M. Monika, I. Carusotto, U. Peschel, and H. M. Price, "Superfluidity of light and its Breakdown in optical mesh lattices," *Phys. Rev. Lett.* **127**(16), 163901 (2021).
- ⁵⁴J. Gea-Banacloche, "Impossibility of large phase shifts via the giant Kerr effect with single-photon wave packets," *Phys. Rev. A* **81**(4), 043823 (2010).
- ⁵⁵J. H. Shapiro, "Single-photon Kerr nonlinearities do not help quantum computation," *Phys. Rev. A* **73**(6), 062305 (2006).
- ⁵⁶J. H. Shapiro and M. Razavi, "Continuous-time cross-phase modulation and quantum computation," *New J. Phys.* **9**(1), 16 (2007).
- ⁵⁷M. Zhang, C. Wang, P. Kharel, D. Zhu, and M. Lončar, "Integrated lithium niobate electro-optic modulators: When performance meets scalability," *Optica* **8**, 652–667 (2021).
- ⁵⁸F. Eltes, C. Mai, D. Caimi, M. Kroh, Y. Popoff, G. Winzer, D. Petousi, S. Lischke, J. E. Ortmann, L. Czornomaz, L. Zimmermann, J. Pompeyrine, and S. Abel, "A BaTiO₃-based electro-optic pockels modulator monolithically integrated on an advanced silicon photonics platform," *J. Lightwave Technol.* **37**(5), 1456–1462 (2019).
- ⁵⁹J. R. Johansson, P. D. Nation, and F. Nori, "QuTiP: An open-source Python framework for the dynamics of open quantum systems," *Comput. Phys. Commun.* **183**, 1760–1772 (2012).
- ⁶⁰D. Hugel and B. Paredes, "Chiral ladders and the edges of quantum Hall insulators," *Phys. Rev. A* **89**, 023619 (2014).
- ⁶¹N. Tomm, S. Mahmoodian, N. O. Antoniadis, R. Schott, S. R. Valentini, A. D. Wieck, A. Ludwig, A. Javadi, and R. J. Warburton, "Photon bound state dynamics from a single artificial atom," *Nat. Phys.* **19**(6), 857–862 (2023).
- ⁶²S. Mahmoodian, G. Calajó, D. E. Chang, K. Hammerer, and A. S. Sørensen, "Dynamics of many-body photon bound states in chiral waveguide QED," *Phys. Rev. X* **10**(3), 031011 (2020).
- ⁶³J.-Q. Liao and C. K. Law, "Correlated two-photon transport in a one-dimensional waveguide side-coupled to a nonlinear cavity," *Phys. Rev. A* **82**(5), 053836 (2010).
- ⁶⁴A. N. Poddubny, "Quasiflat band enabling subradiant two-photon bound states," *Phys. Rev. A* **101**(4), 043845 (2020).
- ⁶⁵O. Firstenberg, T. Peyronel, Q.-Y. Liang, A. V. Gorshkov, M. D. Lukin, and V. Vuletić, "Attractive photons in a quantum nonlinear medium," *Nature* **502**(7469), 71–75 (2013).

- ⁶⁶I. H. Deutsch, R. Y. Chiao, and J. C. Garrison, “Two-photon bound states: The diphoton bullet in dispersive self-focusing media,” *Phys. Rev. A* **47**(4), 3330–3336 (1993).
- ⁶⁷J.-T. Shen and S. Fan, “Strongly correlated two-photon transport in a one-dimensional waveguide coupled to a two-level system,” *Phys. Rev. Lett.* **98**(15), 153003 (2007).
- ⁶⁸V. Venkataraman, K. Saha, and A. L. Gaeta, “Phase modulation at the few-photon level for weak-nonlinearity-based quantum computing,” *Nat. Photonics* **7**, 138–141 (2013).
- ⁶⁹L. Yuan, A. Dutt, M. Qin, S. Fan, and X. Chen, “Creating locally interacting Hamiltonians in the synthetic frequency dimension for photons,” *Photonics Res.* **8**, B8–B14 (2020).
- ⁷⁰M. Zhao and K. Fang, “InGaP quantum nanophotonic integrated circuits with 1.5% nonlinearity-to-loss ratio,” *Optica* **9**, 258–263 (2022).
- ⁷¹J. Lu, M. Li, C.-L. Zou, A. Al Sayem, and H. X. Tang, “Toward 1% single-photon anharmonicity with periodically poled lithium niobate microring resonators,” *Optica* **7**, 1654–1659 (2020).